Molecular Vision 2016; 22:503-517 <http://www.molvis.org/molvis/v22/503>
Received 5 November 2015 | Accepted 15 May 2016 | Published 17 May 2016

Changes in posterior scleral collagen microstructure in canine eyes with an *ADAMTS10* mutation

Craig Boote,[1] Joel R. Palko,[2] Thomas Sorensen,[3] Ashkan Mohammadvali,[4] Ahmed Elsheikh,[4,5] András M. Komáromy,[6,7] Xueliang Pan,[8] Jun Liu[2]

[1]Structural Biophysics Group, School of Optometry and Vision Sciences, Cardiff University, Cardiff, UK; [2]Department of Biomedical Engineering, The Ohio State University, Columbus, OH; [3]Diamond Light Source, Harwell Science and Innovation Campus, Harwell, UK; [4]School of Engineering, University of Liverpool, Liverpool, UK; [5]NIHR Biomedical Research Centre for Ophthalmology, Moorfields Eye Hospital NHS Foundation Trust and UCL Institute of Ophthalmology, UK; [6]Department of Small Animal Clinical Sciences, Michigan State University, East Lansing, MI; [7]Department of Clinical Studies, School of Veterinary Medicine, University of Pennsylvania, Philadelphia, PA; [8]Center for Biostatistics, Department of Biomedical Informatics, The Ohio State University, Columbus, OH

Purpose: We aimed to characterize alterations in the posterior scleral collagen microstructure before detectable disease onset in a canine model of open-angle glaucoma caused by an *ADAMTS10* mutation.
Methods: Collagen orientation, anisotropy degree (proportion of preferentially aligned collagen), and relative density were measured at 0.4 mm spatial resolution using synchrotron wide-angle X-ray scattering. For statistical evaluation of structure parameters, regional averages of the peripapillary and mid-posterior sclera were compared between *ADAMTS10* mutant (affected) dogs (n = 3) and age-matched (carrier) controls (n = 3).
Results: No marked differences in the general pattern of preferential collagen fibril orientation were noted between the control and affected dogs. The peripapillary sclera of all specimens featured strongly aligned circumferential collagen ringing the optic nerve head. Collagen anisotropy was significantly reduced in the mid-posterior sclera of the affected dogs (carrier: 0.27±0.11; affected: 0.24±0.10; p = 0.032) but was not statistically significantly different in the peripapillary sclera (carrier: 0.46±0.15; affected: 0.45±0.17; p = 0.68). Collagen density was statistically significantly reduced in the affected dogs for the mid-posterior sclera (carrier: 28.1±9.14; affected: 18.3±5.12; p<0.0001) and the peripapillary sclera (carrier: 34.6±9.34; affected: 21.1±6.97; p = 0.0002).
Conclusions: Significant alterations in the posterior scleral collagen microstructure are present before the onset of clinical glaucoma in *ADAMTS10* mutant dogs. A reduction in fibrous collagen density is likely an important contributory factor in the previously reported mechanical weakening of the sclera in this model. Baseline scleral abnormalities have the potential to interact with intraocular pressure (IOP) elevations in determining the course of glaucoma progression in animal models of the disease, and potentially in human glaucoma.

Glaucoma is the leading global cause of irreversible blindness and currently affects more than 60 million people worldwide [1]. Although glaucoma risk is evidently multifactorial, there is general agreement that intraocular pressure (IOP) fluctuation plays a central role in the development and progression of the disease [2-4]. Thus, there is potential value in investigating how the mechanical properties of the eye's load-bearing tissues interact with pressure elevations in modulating neuropathy at the optic nerve head (ONH)—a focal point of glaucoma injury [5,6].

The physical effects of IOP on the nerve head axons are mediated through the biomechanical response of the supporting tissues of the eye-wall, predominantly the sclera, the white fibrous tissue that forms 85% of the ocular tunic in humans. Numerical modeling suggests that the biomechanical properties of the posterior sclera are a key factor that determine the magnitude of IOP-derived stresses and strains experienced by optic nerve axons [7-9]. Scleral material properties are, in turn, strongly influenced by the organization of load-bearing type I fibrillar collagen, which forms the bulk of the tissue stroma [10], and there is documented evidence of glaucomatous changes in the collagen structure in the posterior sclera of humans [11-14] and mice [15,16]. However, whether these changes represent baseline difference potentially associated with glaucoma risk or remodeling in response to IOP and/or disease remains largely an open question.

Open-angle glaucoma in the Beagle dog is a well-established spontaneous animal model, caused by autosomal recessive inheritance of a G661R missense mutation of the *ADAMTS10* (Gene ID: 611267, OMIM 608990) gene [17]. In humans, *ADAMTS10* mutations are linked to

Correspondence to: Craig Boote, Cardiff University, School of Optometry and Vision Sciences, Maindy Road, Cardiff CF24 4HQ, UK; Phone: +44 (0)2920 870586. FAX: +44 (0)2920 874859; email: BooteC@cardiff.ac.uk

Table 1. Demographic, genotypic, IOP and tissue thickness data of the Beagle sclera specimens used in the current study.

Dog ID	Sex	Eye	Genotype	Age (months)	IOP at cull (mmHg)	Avg. PPS thickness (mm±S.D.)	Avg. MPS thickness (mm±S.D.)
G66	M	Right	Affected	7	17	0.49 ± 0.05	0.44 ± 0.03
G68	M	Right	Affected	5.6	16	0.39 ± 0.03	0.34 ± 0.07
G70*	M	Right	Affected	5.6	14	0.48 ± 0.09	0.40 ± 0.07
G69	M	Right	Carrier	5.6	16	0.39 ± 0.05	0.32 ± 0.05
G71*	M	Right	Carrier	5.6	13	0.39 ± 0.04	0.33 ± 0.07
G72	F	Right	Carrier	5.6	11	0.39 ± 0.05	0.32 ± 0.06

PPS: peripapillary sclera; MPS: mid-posterior sclera. *Fellow eye used for histological examination of the ONH.

Weill-Marchesani syndrome, a systemic connective tissue disorder that presents with ocular problems, including glaucoma [18]. ADAMTS10 is a secreted metalloproteinase involved in extracellular matrix formation and turnover [19], and we recently showed that the posterior sclera of *ADAMTS10* mutant dogs is more compliant than, and biochemically distinct from, age-matched controls [20]. Importantly, these differences preceded the onset of glaucoma indications. Thus, study of the *ADAMTS10* model offers a useful window on the potential role that baseline scleral abnormalities may play in the pathophysiology of glaucoma. The aim of the current study was to characterize any collagen microstructural changes that occur in the posterior sclera of *ADAMTS10* mutant dogs before the onset of glaucoma is detected.

METHODS

Animals: A colony of Beagle-derived mongrel dogs carrying the G661R *ADAMTS10* mutation was established at the University of Pennsylvania. All animal procedures were approved by the University of Pennsylvania IACUC and performed in accordance with the ARVO Statement for the Use of Animals in Ophthalmic and Vision Research. All dogs were born, raised, and maintained under the same environmental conditions. Three homozygous *ADAMTS10* mutant (affected) dogs and three age-matched heterozygous controls (carriers), all aged between 5 and 7 months old, were used in the current study. Full details of the blood sample genotyping to confirm the pedigree of the animals are published elsewhere [20]. Previous studies have established that homozygous *ADAMTS10* mutant dogs do not develop ocular hypertension at this age [17,21]. However, to confirm the predisease status of the affected animals and the normal control status of the carrier dogs, all animals underwent ophthalmic examination before euthanasia (overdose: ≥85 mg/kg of pentobarbital sodium given intravenously-IV), including indirect ophthalmoscopy, slit-lamp biomicroscopy, and applanation tonometry. In addition, the fellow left eye of one affected (G70) and one carrier (G71) dog was removed for routine histology of the ONH, and this showed no obvious indications of disease in the affected eye. These results are presented in detail in our previous publication [20], while a summary of demographic, genotypic, and IOP data is also shown in Table 1.

Sample preparation and scleral thickness measurement: The right eyes of the euthanized dogs were recovered immediately, and the posterior sclera on the temporal side of the ONH was removed for mechanical testing and biochemical analysis of collagen content, as detailed in our previous publication [20]. Meanwhile, the remaining nasal side of the posterior sclera was preserved in 4% paraformaldehyde for analysis of the collagen microstructure. A custom measurement device, designed and built by the Ocular Biomaterial and Biomechanics Group at the University of Liverpool, was used to measure the scleral thickness. The device consists of a spherical ruby support for mounting tissue in its natural curvature and a vertical height probe positioned 30 mm above the support center point. The probe travels down with a controlled velocity until the probe senses contact with the tissue surface, at which point the traveled distance is used to determine the tissue thickness to an accuracy of 4 µm. For each canine sclera specimen, five repeat measurements were obtained from three sectors of the peripapillary sclera (PPS) and the mid-posterior sclera (MPS), making a total of 15 readings per region per specimen (see Figure 1). For purposes of the scleral thickness measurements and subsequent X-ray scattering analysis, the PPS region was defined as the 2-mm-wide annulus bordering the ONH, while the MPS region was defined as the 2-mm-wide annulus outside the PPS (Figure 1). Average PPS and MPS thickness per specimen is shown in Table 1.

X-ray scattering data collection: Wide-angle X-ray scattering (WAXS) experiments were performed at the Diamond Light Source synchrotron facility (Harwell, UK), using

macromolecular crystallography beamline I02 in a custom-modified fiber-diffraction setup [14,22]. An X-ray beam of wavelength 0.09795 nm, defocused to a cross-sectional diameter of 0.1 mm at the specimen, was used. During X-ray exposure, the sclera specimens were wrapped in polyvinylidene chloride film to limit dehydration, before mounting in Perspex® (Lucite Group Ltd, Southampton, UK) chambers with Mylar® (DuPont-Teijin, Middlesborough, UK) windows. The specimens were mounted such that the tissue retained its natural curvature and the incident X-ray beam was directed perpendicular to the scleral surface at the ONH position. Initial specimen alignment was performed using an in-line microscope, with a central aperture through which the incident beam passed. WAXS patterns resulting from an X-ray exposure of 1 s were recorded on a Pilatus-6MF silicon pixel detector (Dectris Ltd, Baden, Switzerland) positioned 350 mm after the mounted specimen. The specimen was translated between exposures using an integrated motor stage to collect WAXS patterns across each specimen at 0.4 mm (horizontal) × 0.4 mm (vertical) sampling intervals.

X-ray scattering data processing: As previously described, scleral WAXS patterns (e.g., Figure 2A) feature a well-resolved equatorial (i.e., perpendicular to the fiber direction) diffraction peak from the regular 1.6 nm lateral separation of molecular collagen, analysis of which provides averaged information on the amount and direction of type I fibrillar collagen in the scleral tissue volume sampled with the X-ray beam [14,22]. Following this protocol, we obtained three collagen structure parameters from every sampled position in each specimen: 1) the relative number of fibrils preferentially aligned, over and above the underlying isotropic population, as a function of angle within the tissue plane (referred to as

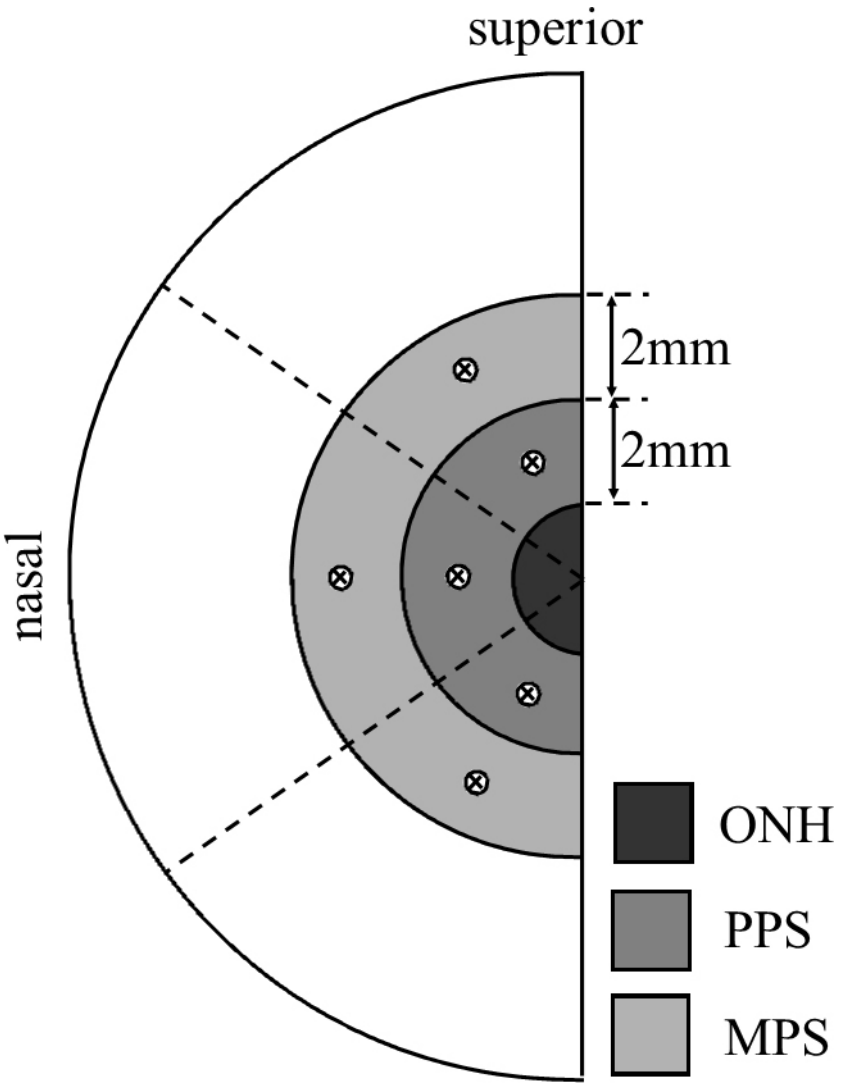

Figure 1. Regional subdivision of posterior canine scleras for statistical evaluation of the collagen structure. ONH = optic nerve head; PPS = peripapillary sclera; MPS = mid-posterior sclera. Crosses denote tissue thickness measurement points (repeated five times per point).

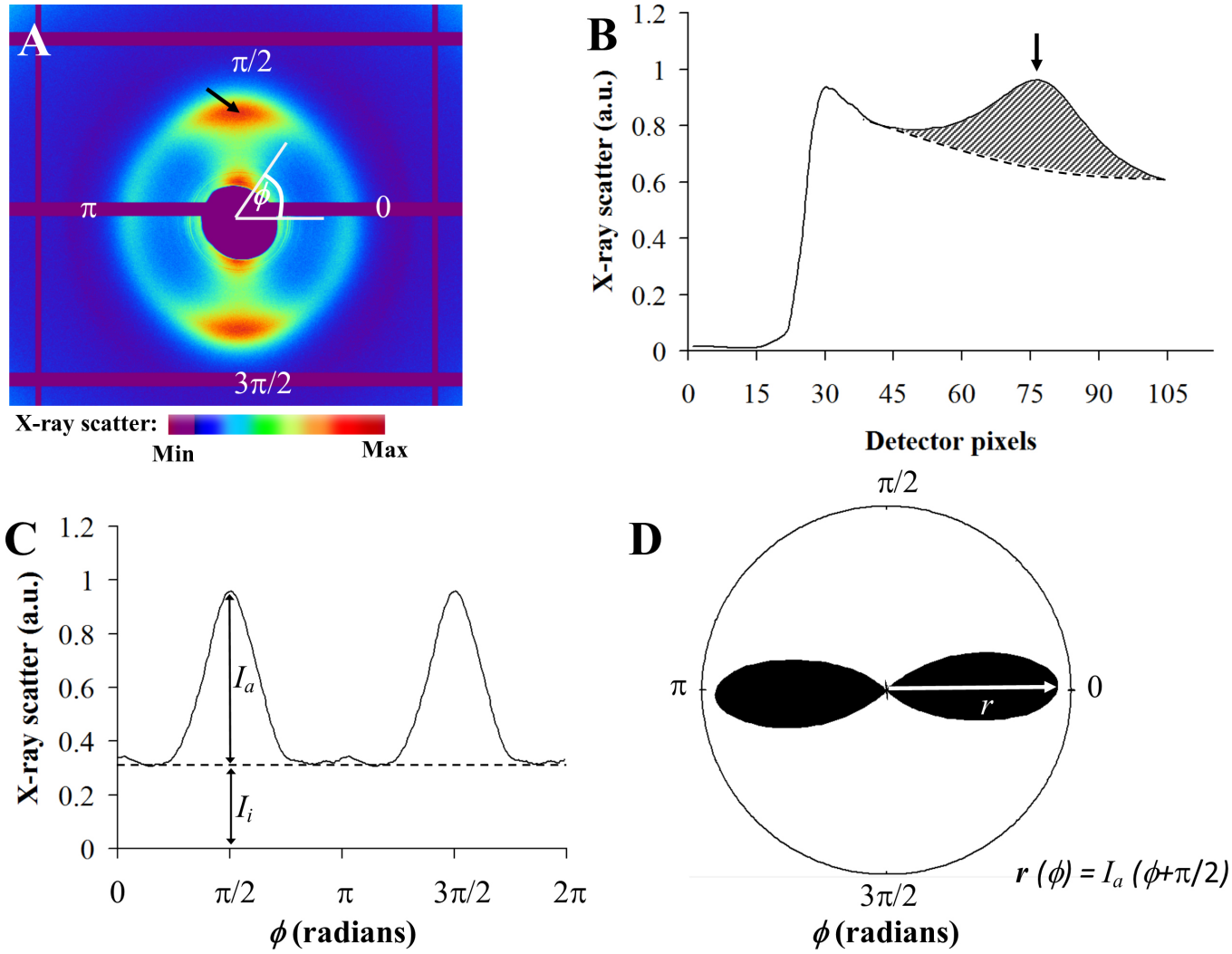

Figure 2. WAXS analysis. **A**: Example wide-angle X-ray scattering (WAXS) pattern from the posterior canine sclera. The spread of intensity as a function of angle ϕ around the collagen intermolecular X-ray scatter peak (arrow) may be analyzed to yield the fibril orientation distribution function. **B**: Power-law background function (broken line) fitted to a radial profile (solid line) through the pattern shown in **A**. A unique background function was independently fitted along 256 equally spaced radial directions for each WAXS pattern. Subtraction of these functions enabled the collagen signal (shaded region) to be extracted in two dimensions. *Arrow:* Collagen peak. **C**: Angular X-ray scatter intensity profile extracted from the pattern shown in **A**. The distribution has two components: scatter arising from isotropic collagen, I_i, and scatter arising from preferentially aligned collagen, I_a. **D**: Collagen orientation distribution plot. The aligned collagen scatter is displayed in polar coordinates, where the length of a vector, ***r***, is proportional to the relative number of collagen fibrils preferentially aligned at angle ϕ.

the "collagen orientation distribution"), 2) the ratio of the preferentially aligned collagen scatter to the total collagen scatter (referred to as the "collagen anisotropy"), and 3) the total collagen scatter divided by the tissue thickness (referred to as the "collagen density").

The raw intensity values were extracted from each WAXS pattern using customized routines running in Optimas 6.5 image analysis software (Media Cybernetics Inc., Marlow, UK) interfaced with Excel (Microsoft, Reading, UK). A custom background-fitting algorithm was then applied to remove scatter from the specimen cell and non-collagen scleral components. Two hundred fifty-six radial profiles originating at the pattern center and ending outside the collagen intermolecular signal were fitted independently with a power-law background function, which was then subsequently subtracted (Figure 2B). The isolated collagen peak was then integrated radially and normalized against fluctuations in X-ray beam current, and the values were extracted to angular bins. The angular profiles were split into isotropic and anisotropic scatter components (Figure

2C) and the latter converted to a polar coordinate system, introducing a π/2 angular shift for equatorial scatter, using Statistica 7 (StatSoft Ltd, Bedford, UK). The collagen orientation distribution function was then displayed as a polar vector plot, in which the line length of a vector at a given angle is proportional to the relative number of preferentially aligned collagen fibrils (Figure 2D). Individual plots were scaled and assigned color codes in Statistica 7, before being assimilated using Excel into montages to visualize the preferred orientation and associated angular distribution of collagen fibrils at each sampled point in the specimen (Figure 3).

Contour maps of collagen anisotropy across each specimen were generated in Excel by computing the ratio of the aligned and total integral collagen scatter values, according to Equation 1:

$$Anisotropy = \frac{\int_0^{2\pi} I_a d\phi}{\int_0^{2\pi} (I_a + I_i) d\phi} \quad (1)$$

where I_a and I_i are the aligned and isotropic components of the collagen scatter, respectively, at angle ϕ. The scleral tissue within a 4 mm radius of the ONH edge (corresponding to the sampled area that had associated scleral thickness measurements) was further analyzed to generate contour maps of relative collagen density, as described by Equation 2:

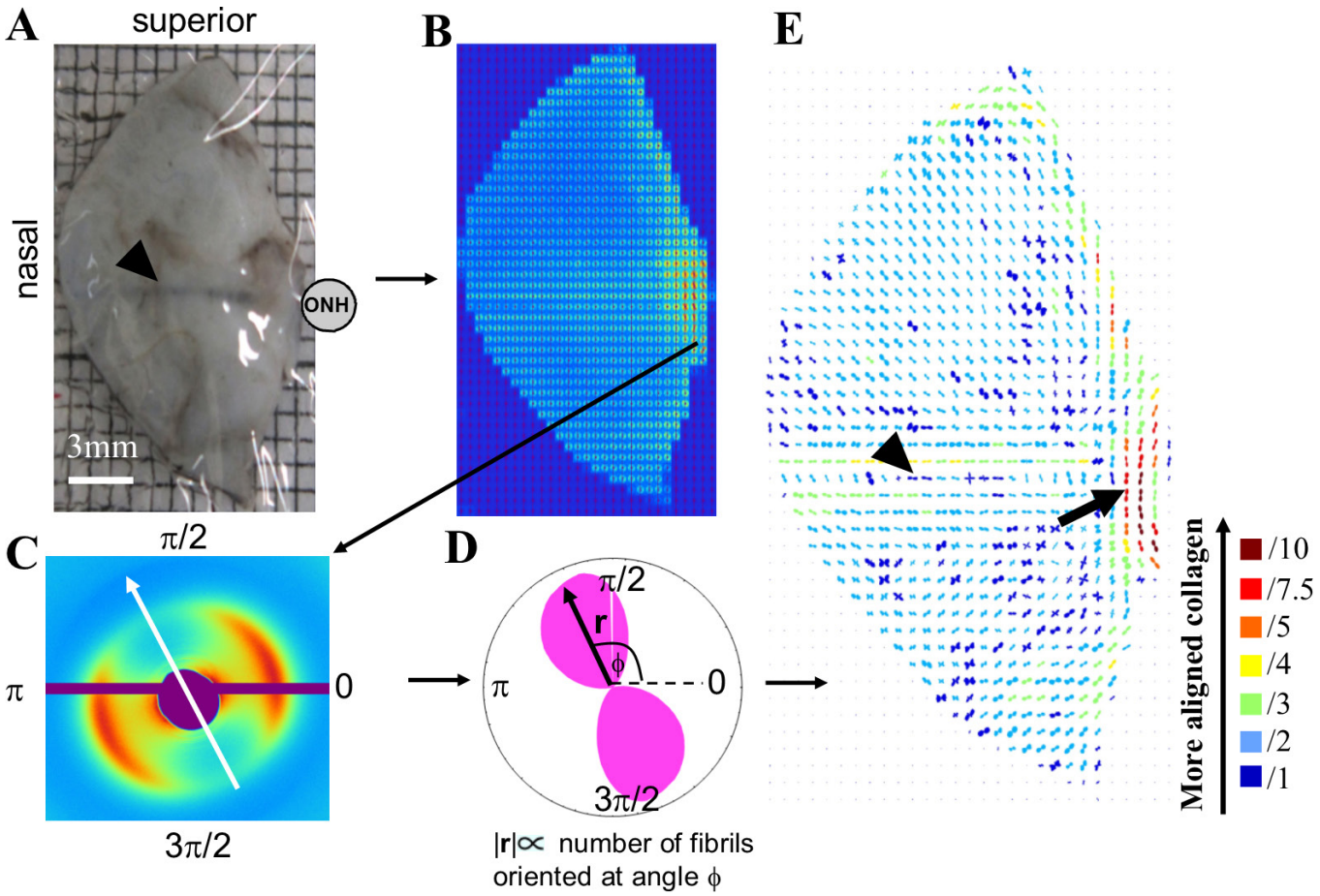

Figure 3. Production of a collagen fibril orientation map. **A**: Photograph of posterior canine sclera specimen G69. *ONH* marks the optic nerve head position. *Arrowhead:* prominent nasal blood vessel (long posterior ciliary artery) is an anatomic landmark of the canine sclera. **B**: Montage of the wide-angle X-ray scattering (WAXS) patterns recorded from the specimen at 0.4 mm spatial resolution. **C**: Expanded view of a WAXS pattern from the peripapillary scleral region. The marked intensity lobing of the collagen intermolecular peak indicates that collagen is preferentially oriented in the direction of the white arrow. **D**: Polar vector plot of collagen orientation distribution extracted from the pattern in **C**. **E**: Montage of polar vector plots showing collagen orientation across the whole specimen. *Arrowhead:* An abrupt change from horizontal to near-vertical collagen demarcates the position of the vessel visible in **A**. *Arrow:* circumferentially oriented collagen, ringing the optic nerve head (ONH), characterizes the peripapillary sclera. The plots have been scaled according to the color key.

$$Density = \frac{\int_0^{2\pi} (I_a + I_i) d\phi}{t} \quad (2)$$

where t is the average local scleral thickness within the MPS or PPS tissue sector that contains the sampled point of interest (see Figure 1).

Statistical analysis: For statistical comparison of the collagen structure in the carrier and affected dog scleras, all anisotropy and density values within the MPS and PPS regions (as defined in Figure 1) were pooled. Linear mixed models for repeated measures were used to compare the differences of collagen anisotropy and density between the carrier and affected dogs. In the mixed models, the regional subdivision (Figure 1) was considered a nested variable, and a variance component covariance structure was used to account for the association of the measures at different regions from the same eye. A major advantage of using mixed models is that this method does not require the same number of data samples collected in each region; in particular, the difference between affected versus carrier or MPS versus PPS can be estimated using the least square means of all data obtained at the same region. The means reported in the paper were based on the least square estimation from the mixed models, while the standard deviations were calculated from the raw data. All mixed model analyses were conducted using the Proc Mixed procedure in SAS version 9.4 (SAS Institute, Cary, NC).

RESULTS

A polar vector map of preferential collagen orientation for carrier specimen G69 is shown in Figure 3E. The shape and color of the individual vector plots indicate that the majority of the nasal posterior sclera was characterized by collagen that is weakly oriented in an approximately radial direction from the ONH. However, a marked exception to this pattern was observed in the peripapillary sclera, where strongly circumferentially aligned collagen was detected (Figure 3E, arrow). In addition, an abrupt shift to near-vertically aligned collagen was detected along the path occupied by the major nasal posterior scleral blood vessel (long posterior ciliary artery; Figure 3A,E, arrowheads), consistent with the helicoidal wrapping of fibrous collagen that reinforces the structure of arterial walls [23]. Figure 4 compares orientation maps from all carrier and affected specimens and shows that there was no marked difference between the two groups in terms of the overall pattern of collagen orientation: The main features were well conserved across all the specimens. To further quantitatively compare the carrier and affected groups, we computed the percentage of vector plots in the PPS and MPS regions that displayed predominantly circumferential, radial, or other orientations to the ONH (Figure 5). These results confirmed the general similarity in collagen orientation between the groups, with the only notable differences being minor changes in the relative proportions of circumferential and radial fibril populations within the MPS region (Figure 5B,D).

Figure 6 presents contour maps of collagen anisotropy (proportion of aligned collagen), which provides validation that collagen alignment was highest in the peripapillary sclera (arrows), corresponding to the region of circumferential collagen. A statistical comparison of anisotropy between regions (Figure 7A) confirmed that anisotropy was, on average, 78% higher ($p = 0.0001$) in the PPS region compared to the MPS region (PPS carrier: 0.46±0.17; PPS affected: 0.45±0.15 versus MPS carrier: 0.27±0.11; MPS affected: 0.24±0.10). Moreover, the marginal (11%) decrease in MPS collagen anisotropy in the affected group was found to be statistically significant ($p = 0.032$) but was not statistically significantly different in the PPS region ($p = 0.68$).

By modulating the total collagen X-ray scatter using the local tissue thickness measurements (Equation 2), we extracted relative measures of fibrillar collagen density in the 4-mm-wide region of the sclera bordering the ONH (Figure 8). A marked visible reduction in collagen density was apparent in all regions of the affected specimens, compared with the carrier controls (Figure 8). Statistical analysis (Figure 7B) confirmed a significant ($p<0.0001$) 39% decrease in PPS collagen density (carrier: 34.6±9.34; affected: 21.1±6.97) and a corresponding 35% decrease in MPS collagen density (carrier: 28.1±9.14; affected: 18.3±5.12). This analysis also revealed that the PPS region was more densely populated with fibrous collagen than the MPS region ($p = 0.0025$). Group average contour maps of collagen anisotropy and density are presented in Figure 9.

DISCUSSION

In this paper, we compared the posterior scleral collagen microstructure of *ADAMTS10* mutant Beagle dogs with normal controls. We found a significant reduction in collagen fibril anisotropy (proportion of aligned collagen) in the mid-posterior sclera of the affected dogs and an accompanying, larger reduction in collagen density in the mid-posterior and peripapillary sclera. These differences were manifested in young dogs before detectable IOP elevations and optic nerve degeneration.

Given that collagen is the main load-bearing component of the ocular tunic, microstructural abnormalities in the

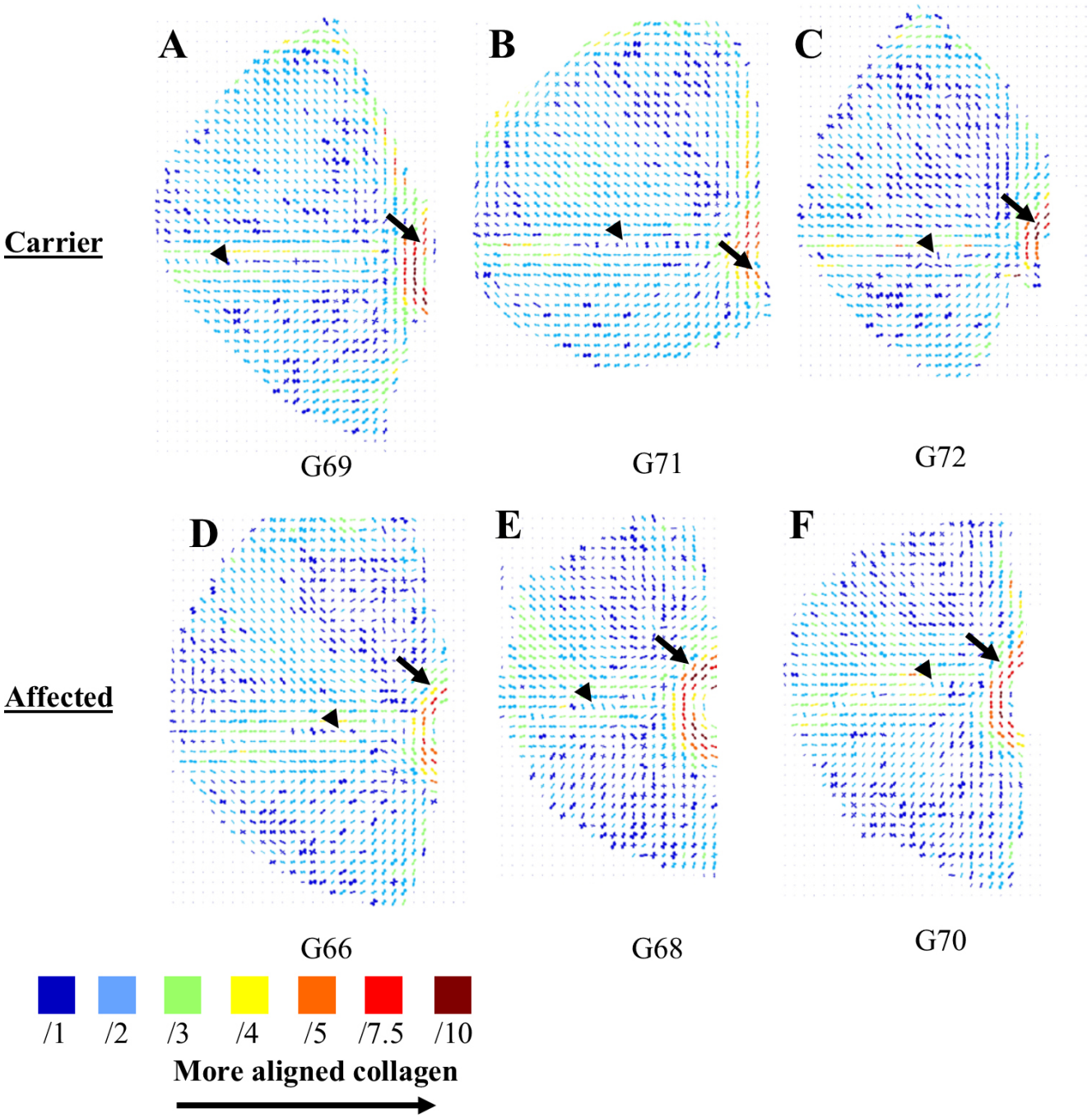

Figure 4. Collagen orientation maps. Polar vector maps of collagen fibril orientation across the (**A**–**C**) carrier and (**D**–**F**) affected *ADAMTS10* mutant posterior canine scleras. Arrowheads and arrows mark the characteristic features associated with the nasal blood vessel (long posterior ciliary artery) and peripapillary collagen annulus, respectively. Data sampling interval: 0.4 mm. The plots have been scaled according to the color key.

sclera could lead to mechanical changes at the macroscopic (tissue) level. Conceivably, these could, in turn, interact with IOP fluctuations and affect the course of glaucoma progression. In a related study [20], we determined that the complex modulus (a measure of overall resistance to deformation) was reduced in the *ADAMTS10* mutant canine sclera and that this correlated with a reduction in insoluble collagen, an indirect measure of collagen crosslinking. The current results provide further evidence that the mechanical weakening of the *ADAMTS10* mutant sclera is related to changes in the

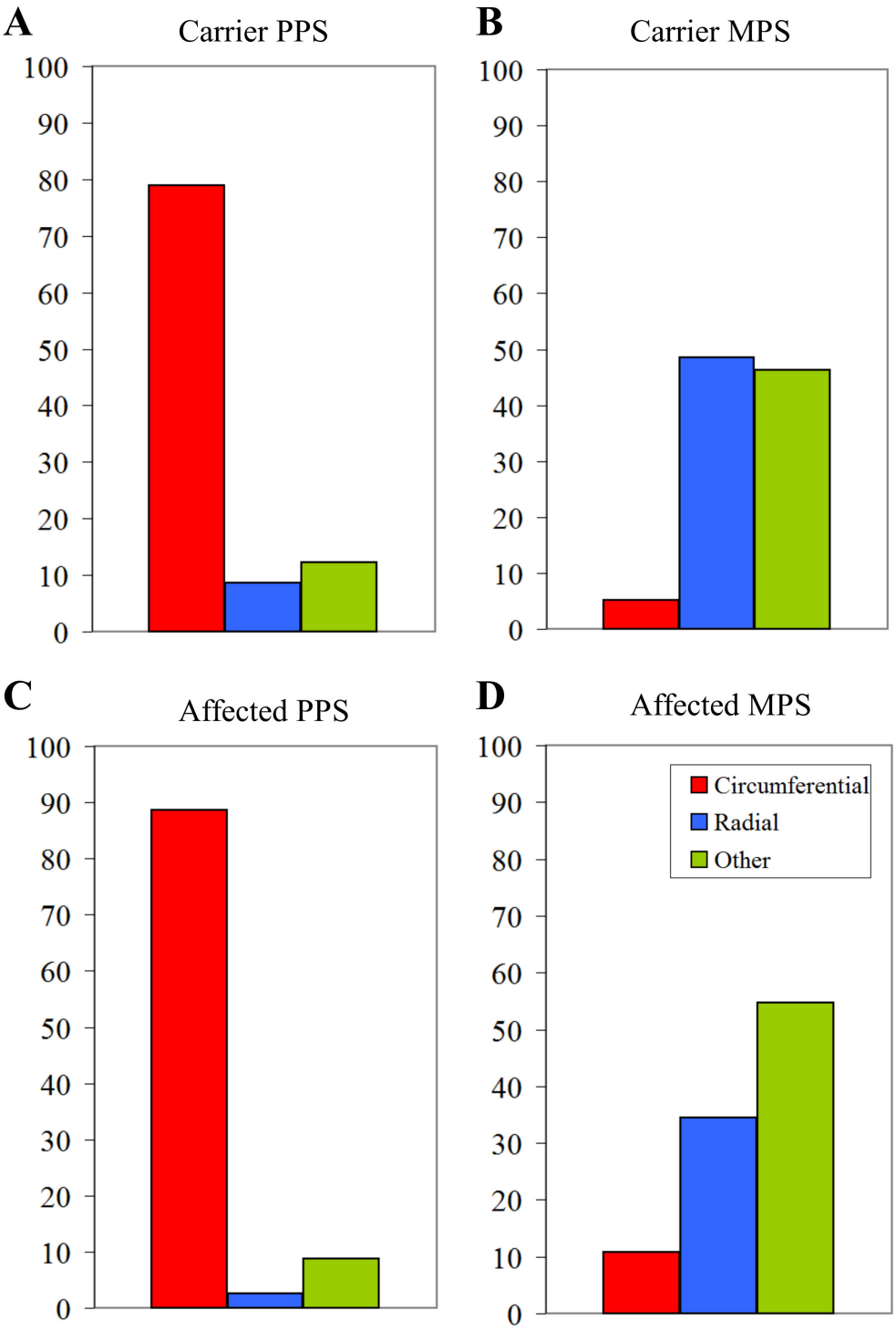

Figure 5. Quantitative comparison of collagen orientation between the (**A**–**B**) carrier and (**C**–**D**) affected *ADAMTS10* mutant posterior canine scleras, showing the average percentage of polar vectors circumferentially, radially, or otherwise oriented (with respect to the optic nerve head) within the peripapillary (PPS) and mid-posterior (MPS) scleral regions.

scleral extracellular matrix, and specifically in the density and organization of fibrillar collagen. Previous research [24-26] has established that scleral collagen orientation is an important factor determining the deformation behavior of the posterior sclera and the ONH to which it lends support. Of particular note is the characteristic collagen annulus that circumscribes the nerve head that was identified previously in humans [13,14,27,28] and rodents [15,29], and is confirmed here for the first time in the canine sclera. Although the peripapillary scleral collagen structure appears well conserved across species, significant variation is observed between the current canine results and data from previous studies in mice

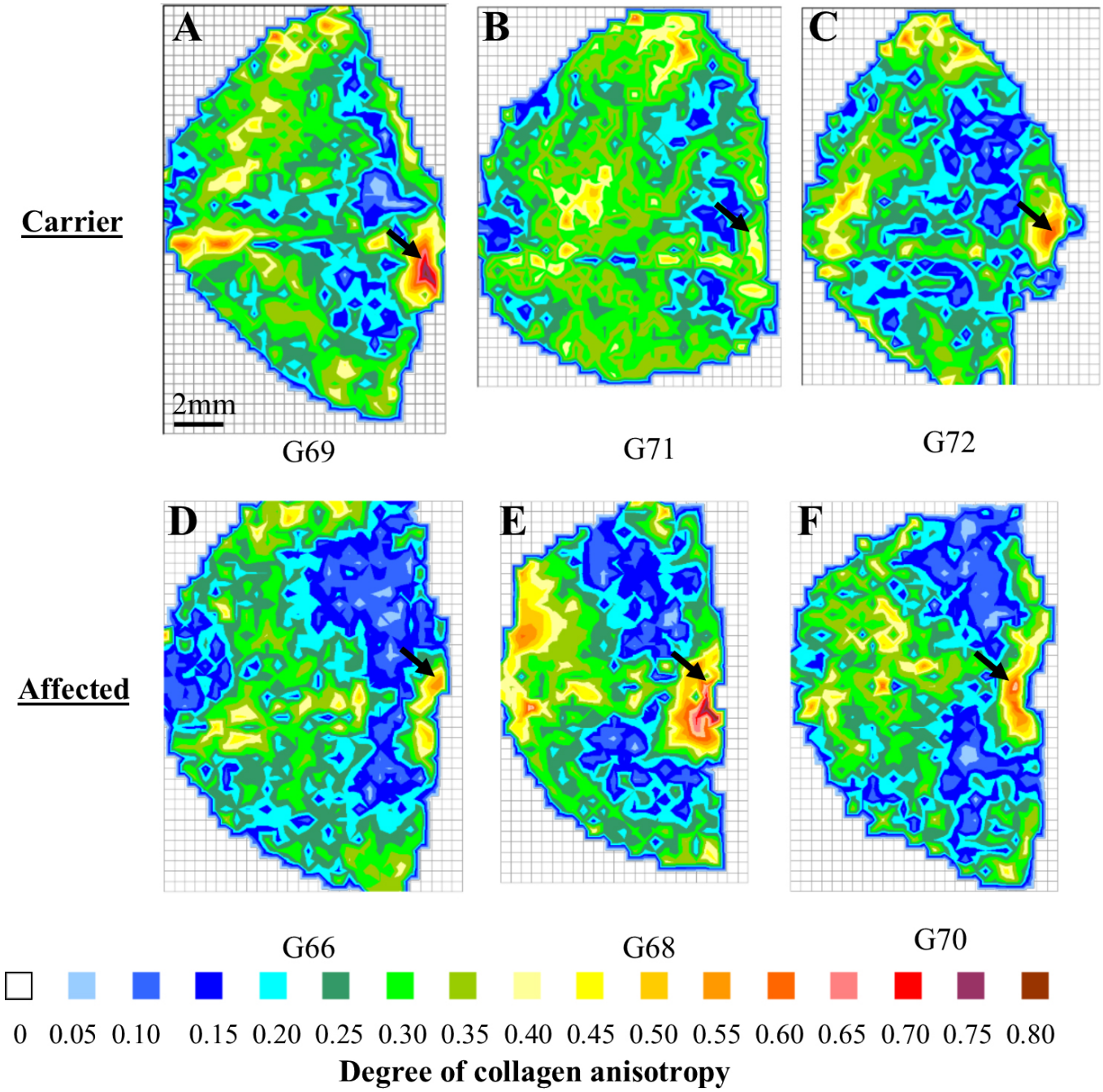

Figure 6. Collagen anisotropy maps. Contour maps of collagen anisotropy (proportion of aligned to total fibrillar collagen) across the (**A**–**C**) carrier and (**D**–**F**) affected *ADAMTS10* mutant posterior canine scleras. A region of maximum anisotropy is observed in the peripapillary sclera (*arrows*). Data sampling interval: 0.4 mm.

[16], rats [29], and humans [14,22,30]. These differences are likely dictated, in part, by inter-species variation in vasculature organization and muscle-insertion locations [22,30].

Computational modeling has shown that the circumferential collagen structure of the peripapillary sclera limits expansion of the scleral canal as IOP is altered [24,31], possibly as a design to shield the ONH from excessive strains. In this context, the subtle changes in collagen anisotropy in the *ADAMTS10* mutant sclera identified in the present study would be expected to have minimal impact on the ONH biomechanics, occurring as they do outside the peripapillary collagen annulus. In contrast, the observed reduction

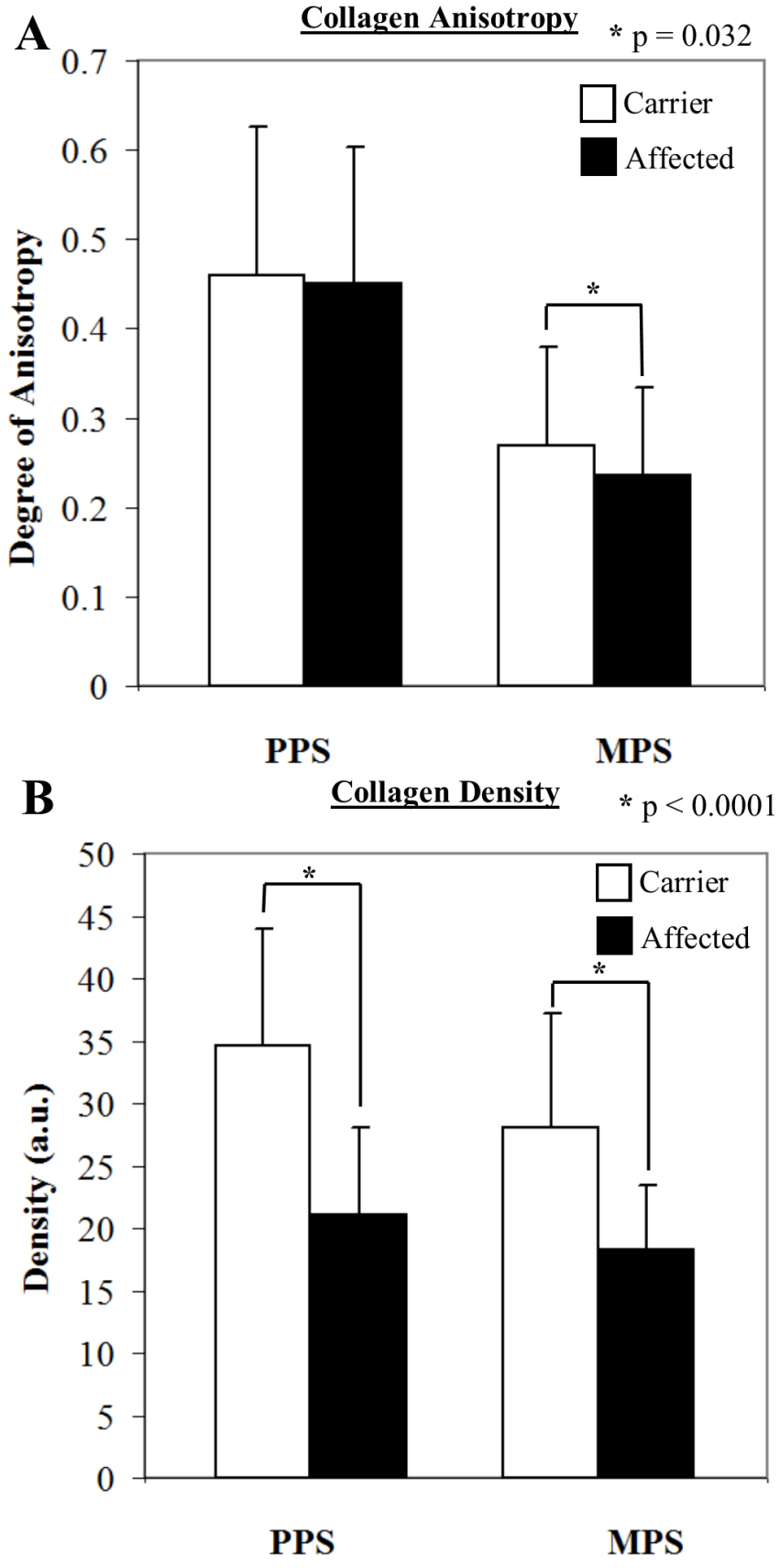

Figure 7. Regional evaluation of the collagen structure. Pooled statistics (linear mixed model for repeated measures) showing comparison of the collagen structure within peri-papillary (PPS) and mid-posterior (MPS) scleral regions between the carrier and affected *ADAMTS10* mutant posterior canine scleras. **A**: A marginal but significant reduction in collagen anisotropy was measured in the mid-posterior scleral region for the affected group. **B**: The marked visible reduction in collagen density within both scleral regions of the affected specimens was statistically confirmed. Error bars: standard deviation.

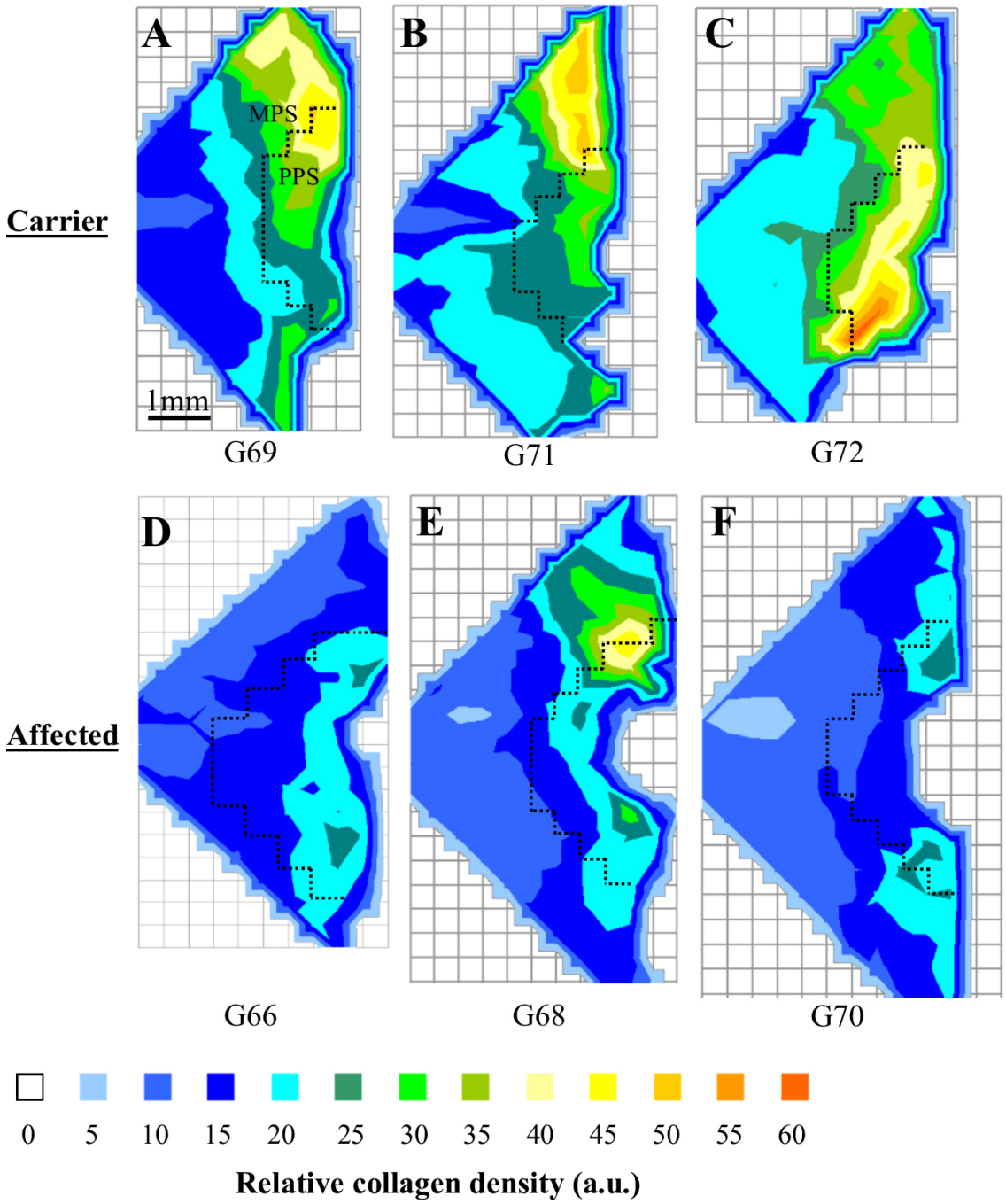

Figure 8. Collagen density maps. Contour maps of relative fibrillar collagen density across the (**A**–**C**) carrier and (**D**–**F**) affected *ADAMTS10* mutant posterior canine scleras. *Broken line:* border of the mid-posterior (MPS) and peripapillary (PPS) scleral regions. Collagen density is visibly reduced in all areas of the affected specimens as compared to carrier controls. Data sampling interval: 0.4 mm.

in collagen density is more likely to affect the mechanical performance of the sclera and, by extension, the nerve head, as they were larger and more widespread, affecting the mid-posterior and peripapillary tissue equally. These observations are consistent with our previous qualitative histological imaging of the *ADAMTS10* mutant canine sclera, in which we reported weaker and less homogeneous histological staining of fibrillar collagen bundles in affected animals [20]. In that study, we also measured the total collagen content of the *ADAMTS10* mutant posterior sclera using biochemical assay and found no significant differences between the heterozygous controls and the homozygous affected specimens [20].

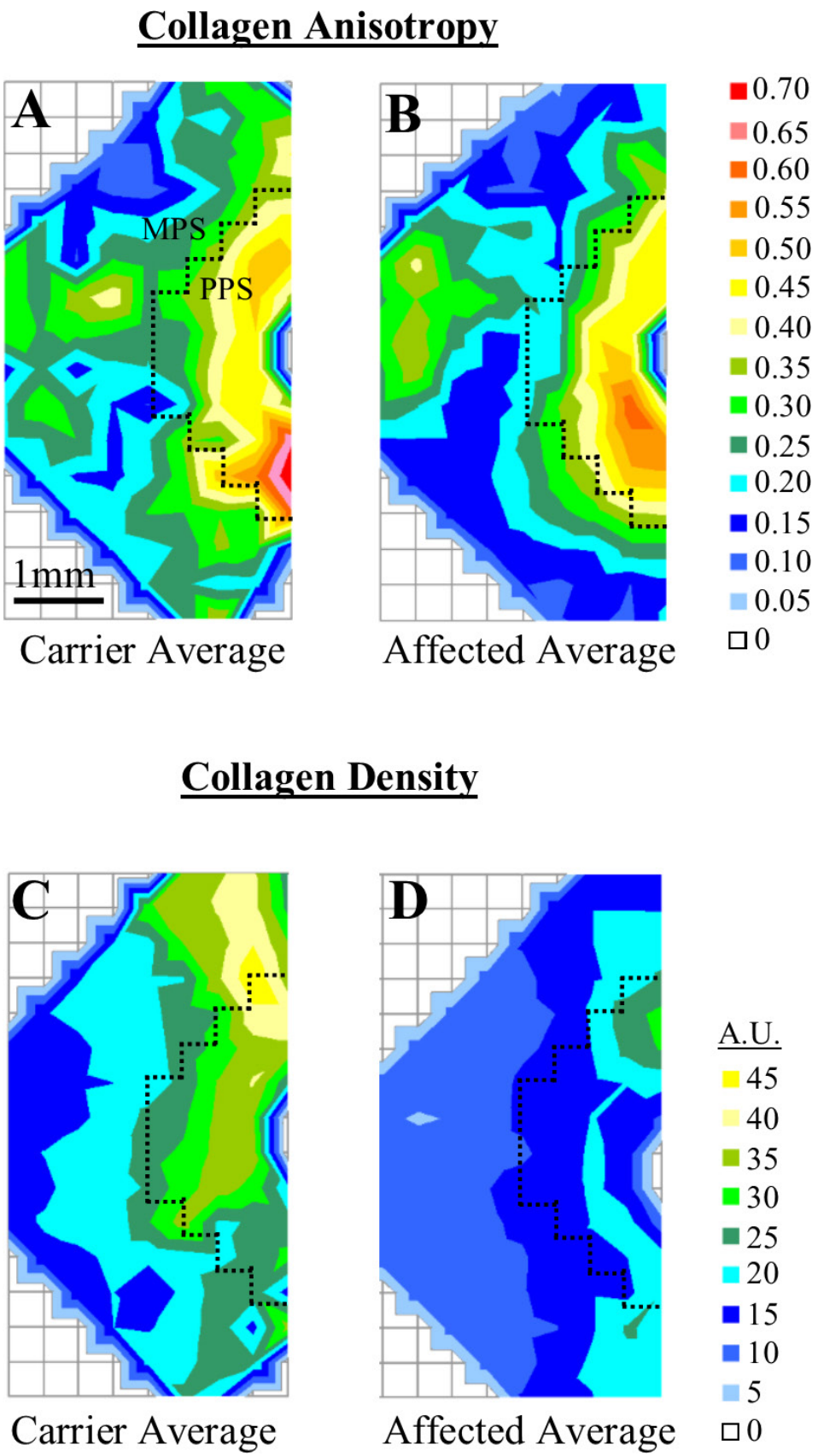

Figure 9. Averaged collagen anisotropy and density maps. Contour maps of fibrillar collagen (**A, B**) anisotropy and (**C, D**) density in the carrier and affected *ADAMTSl0* mutant posterior canine scleras, expressed as group averages. A marked reduction in collagen density in the affected group is again visible. *Broken line:* border of the mid-posterior (MPS) and peripapillary (PPS) scleral regions. Data sampling interval: 0.4 mm.

However, we found that the scleral thickness was higher in affected animals [20], a result confirmed by the present study. Taken together, these previous results are compatible with an overall reduction in collagen density in affected scleras as disclosed by the stromal-averaged X-ray measurements presented here. For a given tissue thickness, lower collagen density would be expected to result in a reduction in scleral mechanical stiffness that, in turn, is predictive of higher tensile strains but potentially reduced posterior bowing in the lamina cribrosa [9]. However, the link between these events and the ultimate clinical outcome of retinal ganglion cell atrophy at the nerve head remains poorly delineated.

From a mechanistic point of view, the cause of the pressure elevation in the *ADAMTS10* mutant dogs likely stems from matrix remodeling-driven compromise of the aqueous drainage apparatus. This is based on the previously reported high level of expression of the ADAMTS10 protein in the trabecular meshwork [17]. However, our current and previous [20] findings of altered scleral properties preceding disease in this model raises the possibility that concomitant abnormalities in structures such as the sclera and the lamina cribrosa may be present at baseline in eyes destined to develop glaucoma that could affect their susceptibility to axonal injury. In light of this, it is interesting that the posterior scleras of individuals of African and European descent (ethnic groups with markedly disparate glaucoma prevalence) have been reported to be structurally and mechanically distinct [32-34].

The current study was subject to some experimental limitations. First, the number of animals available for the study was small (n = 3 per group). However, the structural features and inter-group trends we noted were consistent across the specimens, while by taking a larger number of unique measurements from each specimen and pooling them by region, we were able to achieve an improved statistical power to detect a significant difference by increasing the accuracy and reducing the standard deviations of the measures. Second, variations in tissue hydration within and between specimens may have impacted the collagen scatter intensities, affecting the relative scaling (but not the shape) of the individual vector plots, along with the collagen density measurements. However, as discussed elsewhere, this effect is likely to be minimal when measuring the intermolecular collagen signal [35]. Furthermore, our use of weak paraformaldehyde fixation to preserve the collagen structure may have helped to normalize any hydration variations across the tissue. Third, as we examined the tissue in its natural curvature, the tissue thickness presented to the X-ray beam would have been artificially elevated with increasing distance from the nerve head. This would have led to a proportional increase in total X-ray scatter, and, thus, collagen density. The estimated increase in scatter due to the scleral curvature was calculated to be 3.5% at the extremity of the peripapillary region, increasing to 13% at the outer boundary of the mid-posterior sclera (based on an average Beagle eyeball diameter of 15 mm). The tissue curvature would have affected the collagen density values equally across the specimen groups, specifically overestimating the collagen scatter in the MPS region and consequentially underestimating the difference in collagen density between the MPS and PPS regions. However, the collagen orientation distributions and collagen anisotropy measurements would not have been affected at all since both are thickness-independent [35]. Finally, as the present study included only the nasal side of the posterior sclera, the result trends may not be indicative of the sclera as a whole.

In summary, we have demonstrated reductions in posterior scleral collagen density and fibril anisotropy in dogs with an *ADAMTS10* mutation. These microstructural alterations are likely an important contributory factor in the previously reported mechanical compromise of the sclera in these animals, with the potential to interact with IOP elevations to alter the course of glaucoma progression. The potential link between scleral baseline properties and susceptibility to axonal injury in animal glaucoma models and human disease remains a relatively under-researched aspect of glaucoma pathogenesis that warrants further investigation.

ACKNOWLEDGMENTS

The authors thank Dr Jacek Pijanka, Madara Zile, Martin Spang and Simone Iwabe for technical contributions. This work was supported by Fight For Sight Project Grant 1360 (CB), National Institutes of Health grant NIHRO1EY020929 (JL, XP), The University of Pennsylvania Research Foundation (AMK) and an unrestricted gift from Edward Sheppard and family (AMK).

REFERENCES

1. Tham YC, Li X, Wong TY, Quigley HA, Aung T, Cheng CY. Global prevalence of glaucoma and projections of glaucoma burden through 2040: a systematic review and meta-analysis. Ophthalmology 2014; 121:2081-90. [PMID: 24974815].

2. Bengtsson B, Heijl A. A long-term prospective study of risk factors for glaucomatous visual field loss in patients with ocular hypertension. J Glaucoma 2005; 14:135-8. [PMID: 15741815].

3. Leske MC, Heijl A, Hussein M, Bengtsson B, Hyman L, Komaroff E. Factors for glaucoma progression and the effect of treatment: the early manifest glaucoma trial. Arch Ophthalmol 2003; 121:48-56. [PMID: 12523884].

4. Sommer A, Tielsch JM, Katz J, Quigley HA, Gottsch JD, Javitt J, Singh K. Relationship between intraocular pressure and primary open angle glaucoma among white and black Americans. The Baltimore Eye Survey. Arch Ophthalmol 1991; 109:1090-5. [PMID: 1867550].

5. Anderson DR, Hendrickson A. Effect of intraocular pressure on rapid axoplasmic transport in monkey optic nerve. Invest Ophthalmol 1974; 13:771-83. [PMID: 4137635].

6. Quigley HA, Addicks EM, Green WR, Maumenee AE. Optic nerve damage in human glaucoma. II. The site of injury and susceptibility to damage. Arch Ophthalmol 1981; 99:635-49. [PMID: 6164357].

7. Downs JC, Roberts MD, Burgoyne CF. Mechanical environment of the optic nerve head in glaucoma. Optom Vis Sci 2008; 85:425-35. [PMID: 18521012].

8. Nguyen TD, Ethier CR. Biomechanical assessment in models of glaucomatous optic neuropathy. Exp Eye Res 2015; 14:125-38. [PMID: 26115620].

9. Sigal IA, Ethier CR. Biomechanics of the optic nerve head. Exp Eye Res 2009; 88:799-807. [PMID: 19217902].

10. Watson PG, Young RD. Scleral structure, organisation and disease. A review. Exp Eye Res 2004; 78:609-23. [PMID: 15106941].

11. Coudrillier B, Pijanka JK, Jefferys JL, Goel A, Quigley HA, Boote C, Nguyen TD. Glaucoma-related Changes in the Mechanical Properties and Collagen Micro-architecture of the Human Sclera. PLoS One 2015; 10:e0131396-[PMID: 26161963].

12. Danford FL, Yan D, Dreier RA, Cahir TM, Girkin CA, Vande Geest JP. Differences in the region- and depth-dependent microstructural organization in normal versus glaucomatous human posterior sclerae. Invest Ophthalmol Vis Sci 2013; 54:7922-32. [PMID: 24204041].

13. Jones HJ, Girard MJ, White N, Fautsch MP, Morgan JE, Ethier CR, Albon J. Quantitative analysis of three-dimensional fibrillar collagen microstructure within the normal, aged and glaucomatous human optic nerve head. J R Soc Interface 2015; 12:[PMID: 25808336].

14. Pijanka JK, Coudrillier B, Ziegler K, Sorensen T, Meek KM, Nguyen TD, Quigley HA, Boote C. Quantitative mapping of collagen fiber orientation in non-glaucoma and glaucoma posterior human sclerae. Invest Ophthalmol Vis Sci 2012; 53:5258-70. [PMID: 22786908].

15. Cone-Kimball E, Nguyen C, Oglesby EN, Pease ME, Steinhart MR, Quigley HA. Scleral structural alterations associated with chronic experimental intraocular pressure elevation in mice. Mol Vis 2013; 19:2023-39. [PMID: 24146537].

16. Pijanka JK, Kimball EC, Pease ME, Abass A, Sorensen T, Nguyen TD, Quigley HA, Boote C. Changes in scleral collagen organization in murine chronic experimental glaucoma. Invest Ophthalmol Vis Sci 2014; 55:6554-64. [PMID: 25228540].

17. Kuchtey J, Olson LM, Rinkoski T, Mackay EO, Iverson TM, Gelatt KN, Haines JL, Kuchtey RW. Mapping of the disease locus and identification of ADAMTS10 as a candidate gene in a canine model of primary open angle glaucoma. PLoS Genet 2011; 7:e1001306-[PMID: 21379321].

18. Morales J, Al-Sharif L, Khalil DS, Shinwari JM, Bavi P, Al-Mahrouqi RA, Al-Rajhi A, Alkuraya FS, Meyer BF, Al Tassan N. Homozygous mutations in ADAMTS10 and ADAMTS17 cause lenticular myopia, ectopia lentis, glaucoma, spherophakia, and short stature. Am J Hum Genet 2009; 85:558-68. [PMID: 19836009].

19. Kutz WE, Wang LW, Bader HL, Majors AK, Iwata K, Traboulsi EI, Sakai LY, Keene DR, Apte SS. ADAMTS10 protein interacts with fibrillin-1 and promotes its deposition in extracellular matrix of cultured fibroblasts. J Biol Chem 2011; 286:17156-67. [PMID: 21402694].

20. Palko JR, Iwabe S, Pan X, Agarwal G, Komaromy AM, Liu J. Biomechanical Properties and Correlation With Collagen Solubility Profile in the Posterior Sclera of Canine Eyes With an ADAMTS10 Mutation. Invest Ophthalmol Vis Sci 2013; 54:2685-95. [PMID: 23518772].

21. Peiffer RL Jr, Gum GG, Grimson RC, Gelatt KN. Aqueous humor outflow in beagles with inherited glaucoma: constant pressure perfusion. Am J Vet Res 1980; 41:1808-13. [PMID: 7212410].

22. Pijanka JK, Spang MT, Sorensen T, Liu J, Nguyen TD, Quigley HA, Boote C. Depth-dependent changes in collagen organization in the human peripapillary sclera. PLoS One 2015; 10:e0118648-[PMID: 25714753].

23. Gasser TC, Ogden RW, Holzapfel GA. Hyperelastic modelling of arterial layers with distributed collagen fibre orientations. J R Soc Interface 2006; 3:15-35. [PMID: 16849214].

24. Coudrillier B, Boote C, Quigley HA, Nguyen TD. Scleral anisotropy and its effects on the mechanical response of the optic nerve head. Biomech Model Mechanobiol 2013; 12:941-63. [PMID: 23188256].

25. Girard MJ, Downs JC, Bottlang M, Burgoyne CF, Suh JK. Peripapillary and Posterior Scleral Mechanics-Part II: Experimental and Inverse Finite Element Characterization. J Biomech Eng 2009; 131:051012-[PMID: 19388782].

26. Grytz R, Girkin CA, Libertiaux V, Downs JC. Perspectives on biomechanical growth and remodeling mechanisms in glaucoma Mech Res Commun 2012; 42:92-106. [PMID: 23109748].

27. Morrison JC, Lhernault NL, Jerdan JA, Quigley HA. Ultrastructural Location of Extracellular-Matrix Components in the Optic Nerve Head. Arch Ophthalmol 1989; 107:123-9. [PMID: 2910271].

28. Winkler M, Jester B, Nien-Shy C, Massei S, Minckler DS, Jester JV, Brown DJ. High resolution three-dimensional reconstruction of the collagenous matrix of the human optic nerve head. Brain Res Bull 2010; 81:339-48. [PMID: 19524027].

29. Girard MJ, Dahlmann-Noor A, Rayapureddi S, Bechara JA, Bertin BM, Jones H, Albon J, Khaw PT, Ethier CR. Quantitative mapping of scleral fiber orientation in normal rat

eyes. Invest Ophthalmol Vis Sci 2011; 52:9684-93. [PMID: 22076988].

30. Pijanka JK, Abass A, Sorensen T, Elsheikh A, Boote C. A wide-angle X-ray fibre diffraction method for quantifying collagen orientation across large tissue areas: application to the human eyeball coat. J Appl Cryst 2013; 46:1481-9. .

31. Grytz R, Meschke G, Jonas JB. The collagen fibril architecture in the lamina cribrosa and peripapillary sclera predicted by a computational remodeling approach. Biomech Model Mechanobiol 2011; 10:371-82. [PMID: 20628781].

32. Fazio MA, Grytz R, Morris JS, Bruno L, Girkin CA, Downs JC. Human scleral structural stiffness increases more rapidly with age in donors of African descent compared to donors of European descent. Invest Ophthalmol Vis Sci 2014; 55:7189-98. [PMID: 25237162].

33. Grytz R, Fazio MA, Libertiaux V, Bruno L, Gardiner S, Girkin CA, Downs JC. Age- and race-related differences in human scleral material properties. Invest Ophthalmol Vis Sci 2014; 55:8163-72. [PMID: 25389203].

34. Yan D, McPheeters S, Johnson G, Utzinger U, Vande Geest JP. Microstructural differences in the human posterior sclera as a function of age and race. Invest Ophthalmol Vis Sci 2011; 52:821-9. [PMID: 21051726].

35. Meek KM, Boote C. The use of x-ray scattering techniques to quantify the orientation and distribution of collagen in the corneal stroma. Prog Retin Eye Res 2009; 28:369-92. [PMID: 19577657].

Articles are provided courtesy of Emory University and the Zhongshan Ophthalmic Center, Sun Yat-sen University, P.R. China. The print version of this article was created on 17 May 2016. This reflects all typographical corrections and errata to the article through that date. Details of any changes may be found in the online version of the article.